International Journal for Housing Science and Its Applications
Publish August 5, 2025. Volume 46, Issue 3 Pages 4164-4174

https://doi.org/10.70517/ijhsa463356

Research on multi-channel sensor data fusion and recognition algorithm in laser spot detection

Keya Yuan[1] and Lin Li[2,*]
[1] College of Robotics, Beijing Union University, Beijing, 100101, China
[2] College of Applied Science and Technology, Beijing Union University, Beijing, 100101, China
Corresponding authors: (e-mail: lilin_buu@163.com).

Abstract This paper analyzes the image processing scheme of the capture detector in a spot position detection system based on a four-quadrant detector. Capture unit image by using statistical averaging method for noise template production, combined with the differential shadow method to remove the background noise. The spot center of mass coordinates are obtained to capture the beam. The optimized median filtering scheme, two-dimensional Otsu algorithm are used to process the laser spot image respectively, and then Canny operator is applied to extract the edge of the spot, which achieves the detection and localization of the target spot, and prepares for the initialization of the spot tracking algorithm. The related filtered light spot tracking algorithm is proposed, and the operation process is arranged for it. The spot position detection test conditions are built, and the related filtered spot tracking algorithm is experimentally verified and analyzed. The root-mean-square difference of the correlation filtered spot tracking algorithm for linear and curved trajectories is less than 5 mm, which shows that the correlation filtered spot tracking algorithm expands the detection range of spot position and improves the detection accuracy of spot position without increasing the complexity of the algorithm.

Index Terms spot center of mass, 2D Otsu algorithm, spot tracking algorithm, laser spot image

I. Introduction

Since its birth, laser technology has been widely used in scientific research, industry, medicine, communication and other fields by virtue of its unique advantages such as high brightness, high directivity and high coherence [1], [2]. With the continuous progress of technology, the application range and performance of lasers are also continuously expanding and improving. However, small changes in the laser spot may have a significant impact on the performance of laser applications, so the importance of laser spot detection technology cannot be ignored [3]. In the field of laser processing, the stability of the laser spot directly determines the processing quality and efficiency [4]. For example, in laser cutting and welding, changes in the spot position may lead to inaccurate cutting of materials or degradation of welding quality [5], [6]. In laser marking, deviations in the position of the laser spot may lead to blurred markings or inaccurate positions [7]. Meanwhile, in LIDAR ranging systems, the position of the spot on the target surface directly determines the accuracy and resolution of the measurement, and accurate detection of the laser spot can help the system to more accurately recognize the target and measure the distance, thus improving the overall performance of LIDAR [8]-[10]. Since the stabilization of the laser spot is the basis for achieving a high-quality picture in laser displays, small movements of the spot may lead to distortion or blurring of the picture [11], [12]. Thus, it is crucial to study more accurate, stable and real-time laser spot position detection techniques [13].

This paper analyzes the composition of the spot position detection system based on a four-quadrant detector, which uses normalization and difference algorithms to obtain the initial solution of the spot position, and solves the spot position information from the detector output signals through a digital signal processor. The image collected by the system is used to remove the influence of background noise by applying the differential image method, and the center of mass algorithm is used to calculate the center of mass of the light spot. On the basis of median filtering processing, the two-dimensional Otsu algorithm is used to segment the laser spot image to provide support for spot position detection. Canny operator is applied to extract the edges of the spot to provide a basis for the final spot center position calculation. The correlation filter tracking algorithm is proposed, and the advantages of the correlation filter tracking algorithm are verified by comparing the spot tracking results with the filter CN algorithm.

II. Laser spot detection and localization

II. A. Detector-based spot position detection system

The light spot position detection system based on four-quadrant detector consists of three parts, the front-end is the optical system, the core is the four-quadrant detector, and the back-end is the circuit system as well as the signal processing system. The structure of the light spot position detection system is shown in Fig. 1, in which DSP is the digital signal processor, and A, B, C, and D are the four quadrants of the photosensitive surface.

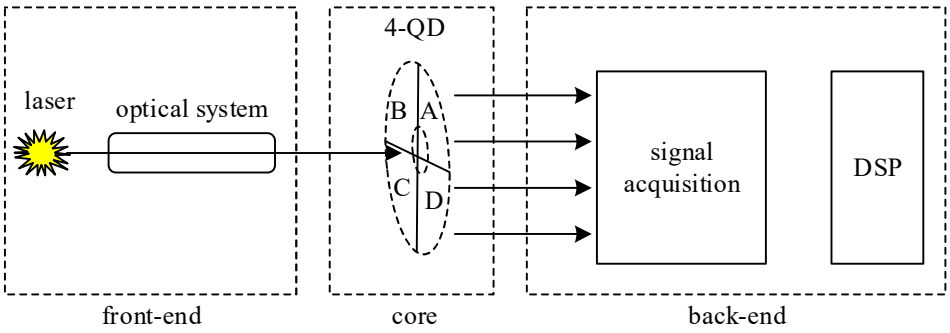

Figure 1: The structure of the detection system of the spot

The optical system consists of a reflection system, a collimation system, an attenuation system, a diaphragm and a focusing system. The optical system allows the detector to adjust the parameters of the incident laser spot, which in turn improves the dynamic range, sensitivity, and accuracy of spot position detection [14].

The four-quadrant detector is also essentially a photodetector that utilizes the photovoltaic effect to convert optical signals into electrical signals and extract information. That is to say, photolithography is utilized to divide a block of photosensitive surface into four quadrants in the Cartesian coordinate system.

When the spot moves on the detector photosensitive surface, the energy of the spot received in each quadrant will change, which leads to a corresponding change in the output photocurrent, so the spot center of mass position can be calculated based on the light energy received in each quadrant. The initial solution of the spot position can be obtained by normalization and difference algorithms:

$$\begin{cases} \partial x = \dfrac{(I_A + I_D) - (I_B + I_C)}{I_A + I_B + I_C + I_D} \\ \partial y = \dfrac{(I_A + I_B) - (I_C + I_D)}{I_A + I_B + I_C + I_D} \end{cases} \tag{1}$$

where $(\delta x, \delta y)$ is the normalized spot center of mass position, $0 \le \delta x \le 1$, $0 \le \delta y \le 1$, and does not represent the actual position of the spot center of mass. The I_A, I_B, I_C, I_D, are the photocurrents in each quadrant of the four-quadrant detector.

The back-end mainly includes the circuit system and the data processing system, which undertake the tasks of detecting, acquiring, transmitting, converting as well as processing the detector output signals. Among them, the circuit system includes transimpedance amplification circuit, pulse detection and acquisition circuit, low-pass filtering circuit, and analog-to-digital conversion circuit. Finally, the spot position information is decoded from the detector output signal by a digital signal processor.

II. B. Capture unit image processing program

II. B. 1) Background noise processing

The task of image processing in the capture phase is to recognize that the beam at the scanning end has been scanned onto the receiving surface at the gazing end. In the actual acquisition, because of the sky background light, atmospheric attenuation and atmospheric turbulence and other factors, resulting in very poor quality of the captured image, low contrast, the target spot is not easy to separate from the background noise, in addition to the sensor's underlying noise on the image signal interference will have a negative impact on the subsequent image processing. In order to more accurately and timely eliminate the background light on the spot information extraction, it is necessary to real-time acquisition of multiple laser irradiation background images to produce real-time background images in line with the actual environment, in order to minimize the impact of the above conditions on the detection accuracy.

In order to reduce the influence of random noise in the background, the method of averaging multiple images acquired for the same scene is adopted. For a noisy image $S(x,y)$, it can be regarded as the sum of the original image $F(x,y)$ and the noise $G(x,y)$ of that image:

$$S(x,y)=G(x,y)+F(x,y) \tag{2}$$

If the random noise $G(x,y)$ superimposed on the image is regarded as non-correlated, then the same target is extracted M times repeatedly under the same background conditions, and then the extracted images are summed. Finally the average of all the images is taken as the output image:

$$\overline{S}(x,y)=\frac{1}{M}\sum_{i=1}^{1}S_i(x,y) \tag{3}$$

The content of random noise in the averaged image $\overline{S}(x,y)$ thus output is greatly weakened compared to the noise content of a single image $S(x,y)$, thus achieving the purpose of smoothing the image.

Since the detector at the gaze end is stationary, statistical averaging is used for noise templating. Before the laser is fired, the number of background samples acquired is N, and each sample image is denoted as $g_i(x,y)$, $i=0,1,2\cdots,N-1$, and the pixel value of each point on the background template map is:

$$T(x,y)=\frac{1}{N}\sum_{i=0}^{N-1}g_i(x,y) \tag{4}$$

The environmental background noise is changed according to each experimental situation, the detector acquired images with normal distribution characteristics of the noise, it is necessary to further transmit the image data to the computer, using digital image processing algorithms to reduce or suppress the noise.

Considering that the background template produced in this paper and the real-time image to be detected are from the images collected by the same detection system, the difference in brightness and gray scale between different images is not very large, and there will be no image reversal, so in this case there is no need to consider the problem of localization matching between the background template and the real-time image. Therefore, by using the difference image method, we can intuitively obtain the spot image excluding the influence of background noise.

Let the background template image be $T(i,j)$, the actual acquired image be $S(i,j)$, and the image after differential shadowing be $D(i,j)$, then we have:

$$D(i,j)=\sum_{j=1}^{M}\sum_{i=1}^{N}\left|S(i,j)-T(i,j)\right| \tag{5}$$

This formula shows the gray level difference between the corresponding pixels of the two images. The background deduction and signal suppression of the images allow the recognition of the captured beams and the accuracy of the measurement of the beam quality parameters to be guaranteed.

II. B. 2) Spot center of mass localization

When a spot is captured by the capture camera, it needs to be localized and compared with the previously calibrated zero point, where the center-of-mass algorithm is used. The center of mass algorithm is based on the principle of finding the center of gravity of a geometric object, and calculates the center of mass of the spot according to the gray value of each pixel on the image.

It can be said that the extraction of the center of mass is a process of integrating the spot signals. Firstly, the surface moments of each discrete signal with respect to the starting point are calculated, and these calculated surface moments are all added together, and finally the integrals of all spot signals on the sensor are calculated, and the quotient of the former and the latter is the position of the center of mass of the spot to be extracted.

Let the spot on the sensor consist of m pixels, $i=1,2,\ldots,m$, each pixel corresponds to the corresponding spatial coordinates x_i,y_i, and its grayscale value is represented by $p_i\left(x_i,y_i\right)$. Let the number of columns of the target surface be the horizontal coordinate and denoted by X, and the number of rows be the vertical coordinate and denoted by Y, for then the center-of-mass coordinate of the spot is:

$$X=\frac{\sum_{i=1}^{m} x_i p_i\left(x_i, y_i\right)}{\sum_{i=1}^{m} p_i\left(x_i, y_i\right)}, Y=\frac{\sum_{i=1}^{m} y_i p_i\left(x_i, y_i\right)}{\sum_{i=1}^{m} p_i\left(x_i, y_i\right)} \tag{6}$$

II. C.Image pre-processing scheme

Image filtering is used to reduce the effect of various noises in the image and improve the quality of the image. Median filtering is a nonlinear filtering technique that can effectively suppress image noise and improve the signal-to-noise ratio, and can effectively remove the pretzel noise in the background. Therefore, the median filtering algorithm is selected in the image processing process.

Median filtering is essentially a statistical ordering filter. For a median filter with a $n \times n$ square window, one sorting requires $n^2\left(n^2-1/2\right)$ comparison operations. It takes a long time to process the images in this system. Therefore, an optimized median filtering scheme is used in this paper, which not only greatly improves its operation speed, but also is easy to be implemented in software.

In this paper, the size of the filtering window is selected as 3×3. The specific method is: to find out the median of the gray value of the pixels in each column of the window, and after that, the median of the middle row is used as the result of the calculation. For the original $n \times n$ sized two-dimensional array, the improved algorithm can simplify it to $n+1$ one-dimensional array containing n pixels. Thus, the number of times needed to perform an operation on the same window is $n\left(n^2-1\right)/2$, which is reduced to the original $1/n$, greatly improving the speed of the operation.

II. D.Laser Spot Image Segmentation

Based on the above processed laser spot image, 2D Otsu algorithm is used to segment the laser spot image to provide support for spot position detection.

The two-dimensional Otsu algorithm is a threshold determination method for image segmentation, which is improved based on Otsu's threshold method. Unlike the one-dimensional Otsu algorithm, the two-dimensional Otsu algorithm takes into account the variation of the gray scale histogram of the image in all directions, and is able to better deal with images with directionality or texture [15], [16].

The basic idea of the two-dimensional Otsu algorithm is to determine the optimal threshold by maximizing the interclass variance to divide the image into foreground and background parts. Unlike the one-dimensional Otsu algorithm, the two-dimensional Otsu algorithm takes into account not only the gray value of the pixel, but also the positional information of the pixel when calculating the interclass variance, which is more suitable for laser spot position detection research.

The output laser spot image is set to be $f(i, j)$, and the spot region and background region probability is calculated as:

$$\begin{cases}\beta_1=\sum_{i=0}^{x} \sum_{j=0}^{x} P(i, j) \\ \beta_2=\sum_{i=x}^{L-1} \sum_{j=x}^{L-1} P(i, j)\end{cases} \tag{7}$$

where β_1 and β_2 denote the probability of the spot region and the background region. The $P(i, j)$ represents the value of the size of the probability that the pixel point (i, j) appears in the light spot region or the background region. The χ denotes the segmentation threshold of the gray value. L is the total value of the gray scale value.

The result of the above equation constructs the formula for calculating the degree of dispersion of the light spot region and the background region, which is expressed as:

$$\xi=\frac{\gamma_1 \beta_1+\gamma_2 \beta_2}{\lambda^o\left(\beta_1^2+\beta_2^2\right)} \tag{8}$$

where ξ denotes the degree of dispersion of the spot region from the background region. The γ_1 and γ_2 denote the weight coefficients of β_1 and β_2. The λ^o denotes the discretization measure standard factor.

When the calculated result of the formula reaches the maximum value, its corresponding χ value is the optimal segmentation threshold, based on which the laser spot image segmentation results are obtained.

II. E. Laser Spot Edge Extraction

Based on the above laser spot image segmentation results, the Canny operator is applied to accurately extract the edges of the spot to provide a basis for the final spot center position calculation.

Canny operator is a commonly used edge detection algorithm in computer vision and image processing, which is widely used in image recognition, feature extraction, target tracking and other tasks, because it can effectively detect the edges of image targets and provide high-quality edge detection results.

The advantage of Canny operator is that it can provide high quality edge detection results and is robust to noise. In addition, the Canny operator has good flexibility in controlling the number of detected edges and edge accuracy by adjusting the parameters.

III. Spot tracking algorithm based on correlation filtering

III. A. Related Filters

In signal theory, the more similar two signals are, the larger their correlation value is, and the design of the correlation filter tracking algorithm comes from this idea. The goal of the correlation filter tracker is to train a filter template h, and using this template to perform a correlation operation with the target image, a regression target can be obtained with one and only one sharp peak g:

$$g = x \otimes h \tag{9}$$

where x denotes the input image, h denotes the correlation filtering template, and g denotes the regression target. The Fourier transform is performed on both sides of the equal sign of Eq. (9), respectively, and the transform to the frequency domain is obtained:

$$\mathrm{F}(g) = \mathrm{F}(x \otimes h) = \mathrm{F}(x) \odot \mathrm{F}(h)^* \tag{10}$$

where $\odot$ refers to the dot product and * refers to the covariance matrix. It is obtained from equation (10):

$$H^* = \frac{G}{X} \tag{11}$$

where H refers to $\mathrm{F}(h)$, G refers to $\mathrm{F}(g)$, and X refers to $\mathrm{F}(x)$.

The filter template h is utilized to perform the correlation operation with the image z to find the response peak Y, and then the time-domain peak y is obtained after Fourier inverse transformation:

$$y = \mathrm{F}^{-1}(Y) = \mathrm{F}^{-1}(H^* \odot Z) \tag{12}$$

where F^{-1} denotes the Fourier inverse transform.

(1) Target characterization

In the classical correlation filtering algorithms MOSSE and CSK algorithms use grayscale features, the characterization ability is weak and can only simply reflect the target information. For this reason this paper proposes a correlation filter tracking algorithm.

(2) Loop Matrix

In the correlation filtering algorithm in the training samples are obtained by the target base sample cycle. The base sample image is represented by the vector $x = [x_1, x_2, \cdots, x_n]^T$, and the cyclic shifting of the base sample image in the horizontal and vertical directions is realized by using the matrices P and Q respectively. $P \times Q$ indicates that the image is cyclically shifted once in the horizontal and vertical directions, respectively. To achieve larger shifts, the multiplication of matrices $P^u \times Q^v$ is used to chain shift x. To wit:

$$P=\begin{bmatrix}0&0&\cdots&0&1\\1&0&\cdots&0&0\\0&1&\cdots&0&0\\\vdots&\vdots&\ddots&\vdots&\vdots\\0&0&\cdots&1&0\end{bmatrix},Q=\begin{bmatrix}0&1&\cdots&0&0\\0&0&\cdots&0&0\\\vdots&\vdots&\ddots&\vdots&\vdots\\0&0&\cdots&0&1\\1&0&\cdots&0&0\end{bmatrix} \tag{13}$$

The new image sample X is obtained from the base sample x after n cyclic shifts, and the matrix X is a $n\times n$ matrix. I.e.:

$$X=C(x)=\begin{bmatrix}x_1&x_2&x_3&\cdots&x_n\\x_n&x_1&x_2&\cdots&x_{n-1}\\x_{n-1}&x_n&x_1&\cdots&x_{n-2}\\\vdots&\vdots&\vdots&\ddots&\vdots\\x_2&x_3&x_4&\cdots&x_1\end{bmatrix} \tag{14}$$

The diagonalization of the matrix X is achieved using the discrete Fourier transform, calculated as follows:

$$X=F\times diag\left(\mathrm{F}\ (x)\right)F^H \tag{15}$$

where F is the discrete Fourier transform matrix, F denotes the Fourier transform, and H refers to the Ermitian matrix.

(3) Ridge regression model

The purpose of sample training for the correlation filtering algorithm is to find a linear regression function $f(x_i)=w^Tx_i$ that minimizes the squared error between the sample x_i and its regression target y_i. The weights w are computed as follows:

$$\min_w\sum_i\left(f(x_i)-y_i\right)^2+\lambda\|w\|^2 \tag{16}$$

where λ denotes the regularization parameter. Bringing $f(x_i)=w^Tx_i$ into Eq. (16) leads to a closed solution:

$$w=\left(X^TX+\lambda I\right)^{-1}X^Ty \tag{17}$$

where the data matrix $X=[x_1,x_2,\cdots,x_n]^T$, the regression target set $y=[y_1,y_2,\cdots,y_n]^T$, and I is the unit matrix. The complex domain of Eq. (17) takes the following form:

$$w=\left(X^HX+\lambda I\right)^{-1}X^Hy \tag{18}$$

where H refers to the Ermitian matrix, * refers to the conjugate matrix, and $X^H=\left(X^*\right)^T$. Bringing Equation (15) to Equation (18), based on the properties of cyclic matrices, one obtains:

$$\mathrm{F}\ (w)=diag\left(\frac{\mathrm{F}\ (x)^*}{\mathrm{F}\ (x)^*\odot\mathrm{F}\ (x)+\lambda}\right)\mathrm{F}\ (y)=\frac{\mathrm{F}\ (x)^*\odot\mathrm{F}\ (y)}{\mathrm{F}\ (x)^*\odot\mathrm{F}\ (x)+\lambda} \tag{19}$$

(4) Fast target detection and model update

The position of the current frame is estimated by extracting a block of image samples at the position of the target in the previous frame, the sample set is processed by cyclic shifting, and filtered by the filter template to find out the sample with the largest peak of the response value, and the corresponding position of the peak point of the response is the position of the target. The response output of the correlation filter is as follows:

$$r=\mathrm{F}^{-1}\left(\mathrm{F}\ \left(\langle\phi(x),\phi(z)\rangle\right)\odot\mathrm{F}\ (\alpha)\right) \tag{20}$$

The Gaussian kernel correlation is expressed as:

$$k^{x,z} = \phi(x)\phi(z)^T = \exp\left(-\frac{1}{\sigma^2}\left(\|x\|^2 + \|z\|^2 - 2\mathrm{F}^{-1}\left(\mathrm{F}(x)^* \square \mathrm{F}(z)\right)\right)\right) \tag{21}$$

In order to improve the immunity of the algorithm to interference, the correlation filter is updated using linear interpolation to update the filter model. The updated method is as follows:

$$\begin{cases} x_t = (1-\eta)x_{t-1} + \eta x_t \\ \alpha_t = (1-\eta)\alpha_{t-1} + \eta\alpha_t \end{cases} \tag{22}$$

where x_t refers to the target model for the current frame, α denotes the model coefficients, and η denotes the learning rate.

III. B. Correlation Filter Tracking Algorithm Flow

The previous subsection introduced the important components of the correlation filtering algorithm, which is mainly divided into three processes to complete the tracking: preprocessing, detection, training and updating. Among them, the preprocessing process is responsible for extracting the target features and generating the filter template. The detection process is responsible for estimating the target position. The updating and training processes are mainly responsible for generating more robust filter templates. The specific steps of the algorithm to realize tracking are as follows:

Step 1: Initialization, based on the target position of the given initial frame, extract the sample block, extract the image features using feature descriptors, and generate the training sample set using the loop matrix.

Step 2: Train the classifier using the sample set and generate the filter template.

Step 3: Input the next frame of image, extract the image block of the current frame and perform correlation operation with the filter template to calculate the position with the largest response peak which is the target position.

Step 4: Perform template and coefficient update according to equation (22).

Step 5: Repeat step 3 until all frames are read.

III. C. Experimental results and analysis

III. C. 1) Experimental conditions

Experimental platform parameters: the system is 64-bit win10 home edition, programming bad MATLAB R2021b, processor Intel i7-8th, the main frequency of 2.3GHz, memory 8G.

The collected video input of two groups of moving light spots with different motion trajectories (linear and curved) is used as the video source, which is processed by the algorithm for output, and the algorithm results are obtained.

The CN algorithm in this paper still adopts the original CN parameters, the standard deviation of the Gaussian kernel σ is 0.3, the regularization coefficient λ is 0.03, and the learning factor η is 0.05. The CN algorithm adopts the color name feature, which refines the RGB color feature, and is capable of reflecting the color information of the target. The filter parameters are set as follows:

$$State\ transfer\ matrix\ A = \begin{bmatrix} 1\ 0\ t\ 0\ 0.5t^2\ 0 \\ 0\ 1\ 0\ t\ 0\ 0.5t^2 \\ 0\ 0\ 1\ 0\ t\ 0 \\ 0\ 0\ 0\ 1\ 0\ t \\ 0\ 0\ 0\ 0\ 1\ 0 \\ 0\ 0\ 0\ 0\ 0\ 1 \end{bmatrix} \tag{23}$$

$$Observation\ equation\ h = \begin{bmatrix} \sqrt{Z(1)^2 + Z(2)^2} \\ \tan^{-1}\left(Z(2)/Z(1)\right) \end{bmatrix} \tag{24}$$

Estimate the noise covariance matrix:

$$Q = diag\left[10\ 0.1\ 0.1\ 0.1\ 0.1\right] \tag{25}$$

$$\Delta Q = diag\left[1\ 1\ 0.01\ 0.01\ 0.01\right] \tag{26}$$

State Vector:

$$X_i = \begin{bmatrix} x_k & y_k & \square & \square & \square & \square \end{bmatrix}^T \quad (27)$$

Measurement Vector:

$$Z_k = \begin{bmatrix} x_k & y_k \end{bmatrix}^T \quad (28)$$

III. C. 2) Experimental results

In order to verify the effectiveness of the algorithm (correlation filter tracking algorithm) in this paper, it is designed to take the sinusoidal trajectory as the target's actual motion trajectory, increase the Gaussian white noise as the motion trajectory measurement, and carry out simulation experiments for comparative validation to test the performance of the two filtering algorithms.

The comparison of tracking results is shown in Fig. 2, Fig. (a) is 1000 filtering cycles and Fig. (b) is 5000 filtering cycles.

The state estimation E of this paper's algorithm is smaller than that of the filter CN algorithm, and the absolute error in a single filtering cycle tends to converge. At the beginning of the simulation, the state estimation accuracy of the two algorithms is comparable, but as the filtering algorithm continues, the state estimation accuracy of this paper's algorithm is high and stabilizes.

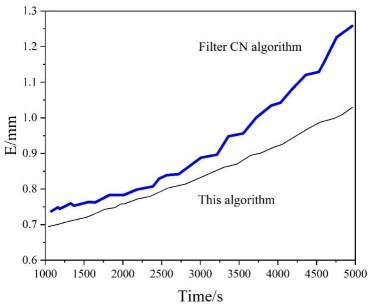

(a) 1000 filter cycles

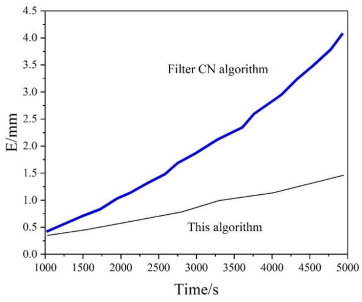

(b) 5000 filter cycles

Figure 2: Tracking effect comparison

The accuracy of the tracking was measured using the root mean square error. The tracking results from frame 130 to 180 of the linear trajectory video and from frame 100 to 170 of the curved trajectory video are analyzed. The tracking results for different frames are shown in Fig. 3, Figs. (a) and (b) are linear-like (left to right) and curved (right to left), respectively.

As can be seen from the figures, the filter CN algorithm tracking frame drifts after the light spot disappears and the tracking fails. The traditional algorithm tracking frame converges to the algorithm estimate and the tracking fails. In this paper, the algorithm uses linear interpolation to update the filter model, and the tracking frame is centered on the optimal estimate, continues to search for the target, and successfully captures and continues to track the target when it reappears.

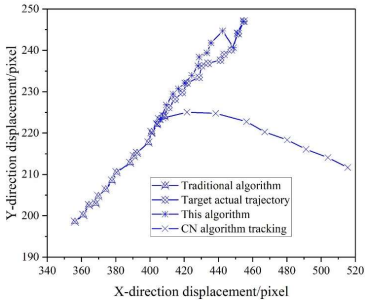

(a) 130 to 180

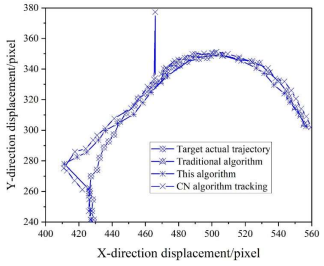

(b) 100 to 170

Figure 3: Trace results of different frames

The comparison of the root mean square error of the algorithm tracking results is shown in Table 1. The root-mean-square error of the tracking results of the filter CN algorithm is better than the root-mean-square error of the tracking results of the traditional algorithm. However, whether it is a linear trajectory or a curved trajectory, the algorithm in this paper outperforms the two comparative algorithms, and controls the root-mean-square difference of the spot tracking results within 5 mm.

Table 1: Algorithm tracking results mean and mean/mm

	Test frequency	CN algorithm	Traditional algorithm	This algorithm
Linear trajectory	Test 1	136.581	12.364	1.521
	Test 2	139.152	12.118	1.236
	Test 3	135.121	13.024	1.334
	Test 4	133.496	13.252	1.259
	Test 5	134.254	12.698	1.568
Curve trajectory	Test 1	402.694	97.513	4.692
	Test 2	410.302	98.241	4.125
	Test 3	405.787	96.325	3.948
	Test 4	406.962	96.554	3.251
	Test 5	408.554	97.127	4.527

III. C. 3) Mass center extraction results

The multi-channel sensor collects the laser spot information scattered on the surface of the measured object through the optical system, and the image acquisition card transmits the spot information to the computer for processing, so as to get the digitized information of the surface shape of the measured object. The system calibration and measurement processes are carried out on the optical platform, which has been vibration isolation and other measures to minimize the interference of external factors.

The static targets on the experimental platform are measured several times at different distances, and the images are captured at the near point of measurement, the far point of measurement, and the intermediate position in between, and 500 frames of images are taken. An arbitrary line was taken to calculate the gray scale distribution, and the gray scale distribution curve of the image is shown in Fig. 4, which is approximated as Gaussian distribution.

During the measurement process, a large amount of photoelectric noise is mixed in the target image due to environmental factors, optical system and other influences. The noise can be shielded by setting the threshold value to retain the effective target information.

The selection of the threshold size is critical, the threshold is too small, the window is large, the target image will also be mixed with too much noise, affecting the measurement accuracy. Threshold selection is too large, the window is small, in the filtering of noise at the same time will make the target image information lost part of the image, resulting in a reduction in the effective image information, also affect the measurement accuracy. Therefore, selecting a suitable threshold value can improve the accuracy of the measurement results.

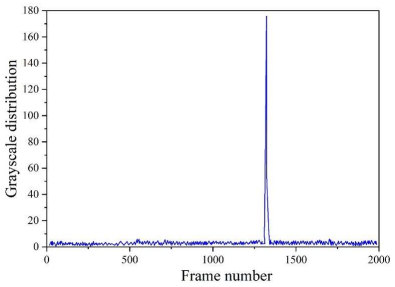

Figure 4: Image grayscale distribution curve

The center of mass extraction of the light spot is performed using the gray scale center of mass method with different thresholds for the acquired images in the middle position, and the light spot center of mass results are calculated. The light spot center of mass extraction results of the grayscale center of mass method are shown in Fig. 5.

It is found by studying the graph that the position of the spot center of mass increases with the increase of the selected threshold value. This is caused by the asymmetric distribution of the light spot and the standard value

increases with the increase of the selected threshold value. This is due to the fact that the increase in the selected threshold value causes a decrease in the effective pixel information of the target and a decrease in the accuracy resolution.

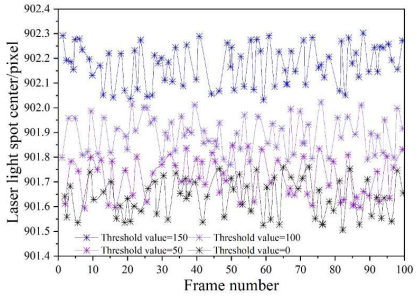

Figure 5: The results of the qualitative center of grayscale mass center

The calculated results of the gray scale center of mass method spot mass center extraction method mentioned above were statistically analyzed, and the mean, standard deviation and limiting error were calculated respectively.

The spot center of mass extraction results of the grayscale center of mass method are compared with the spot center of mass extraction results of the curve fitting method. The statistics of the spot center of mass extraction results of the two methods are shown in Table 2. The limiting errors of the spot center of mass extraction results of the grayscale center of mass method are 0.21~0.26, while the limiting errors of the curve fitting method are 0.1~0.15, which are lower than that of the grayscale center of mass method. The curve fitting method has small fluctuation, within 0.05 pixels, and has the highest localization accuracy and remains basically unchanged. However, due to the complexity of its algorithm, which usually requires a large number of operations, its practicality in the field of real-time high-speed on-line inspection has received great limitations, and there is not much use value, so this paper did not choose this algorithm.

Table 2: The results of the results of the two methods were calculated

Method	Statistical result	Threshold value=0	Threshold value=50	Threshold value=100	Threshold value=150
Grayscale center method	Mean value	905.63	905.52	905.94	906.25
	Standard deviation σ	0.05	0.06	0.05	0.07
	Limit error 3σ	0.26	0.23	0.21	0.22
Curve fitting	Mean value	905.89	905.91	905.15	905.76
	Standard deviation σ	0.03	0.04	0.04	0.05
	Limit error 3σ	0.13	0.15	0.10	0.12

IV. Conclusion

In this paper, the spot position detection system with four-quadrant detector is utilized to obtain the spot position image, preprocess the spot image, and calculate the spot tracking results with the proposed correlation filter tracking algorithm.

The filter CN algorithm is selected to compare the tracking results with the algorithm of this paper (correlation filter tracking algorithm). The reason for selecting the filter CN algorithm is that the CN features are used in the filter CN algorithm to enhance the description of the color, reduce the effect of illumination, and achieve the recognition of the pixel point. In the light spot tracking results, it is found that as the filter algorithm continues, the state estimation accuracy of this paper's algorithm is higher and stabilized. After the light spot disappears, the filter CN algorithm tracking frame drifts and the tracking cannot proceed. The root-mean-square difference of this paper's algorithm's tracking of linear trajectories is 1.2 mm to 1.6 mm, which is significantly lower than that of the filter CN algorithm. The size of the threshold value affects the measurement accuracy, and the position of the spot center of mass increases with the selected threshold value. However, the gray scale center of mass method is more suitable for the system in this paper when the thresholds are 0, 50, 100, and 150, respectively, and the standard deviation σ is 0.05~0.07.

Funding

This work was supported by National Key Research and Development Program of China in 2022 (Grant No. 2022YFB4601100).

References

[1] Liu, H., Lin, W., & Hong, M. (2021). Hybrid laser precision engineering of transparent hard materials: challenges, solutions and applications. Light: Science & Applications, 10(1), 162.
[2] König, K. (2023). Medical femtosecond laser. Journal of the European Optical Society-Rapid Publications, 19(2), 36.
[3] Zhu, J., Xu, Z., Fu, D., & Hu, C. (2019). Laser spot center detection and comparison test. Photonic Sensors, 9, 49-52.
[4] Sugioka, K. (2017). Progress in ultrafast laser processing and future prospects. Nanophotonics, 6(2), 393-413.
[5] Feng, J., Wang, J., Zhao, X., Liu, Z., & Ding, Y. (2024). Laser weld spot detection based on YOLO-weld. Scientific Reports, 14(1), 29403.
[6] Colom, M., Rodríguez-Aseguinolaza, J., Mendioroz, A., & Salazar, A. (2021). Sizing the depth and width of narrow cracks in real parts by laser-spot lock-in thermography. Materials, 14(19), 5644.
[7] Xuan, W., Xiuqin, S., Guizhong, L., Junfeng, H., & Rui, W. (2020). Investigation of high-precision algorithm for the spot position detection for four-quadrant detector. Optik, 203, 163941.
[8] Benedek, C., Majdik, A., Nagy, B., Rozsa, Z., & Sziranyi, T. (2021). Positioning and perception in LIDAR point clouds. Digital Signal Processing, 119, 103193.
[9] Pawar, K. S., Teli, S. N., Shetye, P., Shetty, S., Satam, V., & Sahani, A. (2022). Blind-spot monitoring system using LiDAR. Journal of The Institution of Engineers (India): Series C, 103(5), 1071-1082.
[10] Radwell, N., Selyem, A., Mertens, L., Edgar, M. P., & Padgett, M. J. (2019). Hybrid 3D ranging and velocity tracking system combining multi-view cameras and simple LiDAR. Scientific reports, 9(1), 5241.
[11] Bonnett Del Alamo, M., Soncco, C., Helaconde, R., Bazo Alba, J. L., & Gago, A. M. (2021). Laser spot measurement using simple devices. AIP Advances, 11(7).
[12] Li, H., Andreev, M. V., Panchenko, Y. N., & Puchikin, A. V. (2022). Improving the stability of the optical system of a laser source based on a position-sensitive detector. Atmospheric and Oceanic Optics, 35(5), 615-619.
[13] Vázquez-Otero, A., Khikhlukha, D., Solano-Altamirano, J. M., Dormido, R., & Duro, N. (2016). Laser spot detection based on reaction diffusion. Sensors, 16(3), 315.
[14] Noor Wisam Sabri,Firas S. Mohammed & Asmaa A. Abdul Razaq. (2025). Wavelength division multiplexing of free space optical system under the effect of oil fire smoke. Journal of Optical Communications,46(2),405-412.
[15] Xun Ma,Kai Liu,Anlei Liu,Xuchao Jia & Yong Wang. (2022). Classification Method for Power Load Data of New Energy Grid based on Improved OTSU Algorithm. International Journal of Advanced Computer Science and Applications (IJACSA),13(10).
[16] Ren Honge,Zhou Yang & Zhu Meng. (2016). Tree Image Segmentation Based on an Improved Two-Dimensional Otsu Algorithm. International Journal of Hybrid Information Technology,9(9),199-210.